BIOCHEMISTRY
including biophysical chemistry & molecular biology

Article

pubs.acs.org/biochemistry

Oxidation-Induced Conformational Changes in Calcineurin Determined by Covalent Labeling and Tandem Mass Spectrometry

Xiao Zhou,[†] Caitlin Mester,[†] Paul M. Stemmer,[‡] and Gavin E. Reid*[,†,§]

[†]Department of Chemistry, and [§]Department of Biochemistry and Molecular Biology, Michigan State University, East Lansing, Michigan 48824, United States

[‡]Institute of Environmental Health Science, Wayne State University, Detroit, Michigan 48201, United States

Supporting Information

ABSTRACT: The Ca^{2+}/calmodulin activated phosphatase, calcineurin, is inactivated by H_2O_2 or superoxide-induced oxidation, both *in vivo* and *in vitro*. However, the potential for global and/or local conformation changes occurring within calcineurin as a function of oxidative modification, that may play a role in the inactivation process, has not been examined. Here, the susceptibility of calcineurin methionine residues toward H_2O_2-induced oxidation were determined using a multienzyme digestion strategy coupled with capillary HPLC−electrospray ionization mass spectrometry and tandem mass spectrometry analysis. Then, regions within the protein complex that underwent significant conformational perturbation upon oxidative modification were identified by monitoring changes in the modification rates of accessible lysine residues between native and oxidized forms of calcineurin, using an amine-specific covalent labeling reagent, *S*,*S*′-dimethylthiobutanoylhydroxysuccinimide ester (DMBNHS), and tandem mass spectrometry. Importantly, methionine residues found to be highly susceptible toward oxidation, and the lysine residues exhibiting large increases in accessibility upon oxidation, were all located in calcineurin functional domains involved in Ca^{2+}/CaM binding regulated calcineurin stimulation. These findings therefore provide initial support for the novel mechanistic hypothesis that oxidation-induced global and/or local conformational changes within calcineurin contribute to inactivation via (i) impairing the interaction between calcineurin A and calcineurin B, (ii) altering the low-affinity Ca^{2+} binding site in calcineurin B, (iii) inhibiting calmodulin binding to calcineurin A, and/or (iv) by altering the affinity between the calcineurin A autoinhibitory domain and the catalytic center.

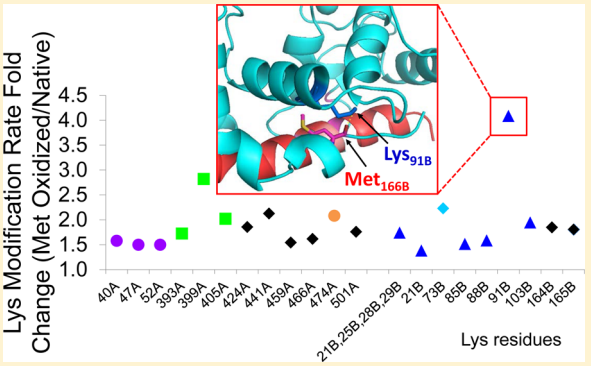

INTRODUCTION

Calcineurin (CN) is a Ca^{2+}/calmodulin (CaM) activated serine/threonine phosphatase that is widely distributed in mammalian tissues.[1] CN functions in signal transduction pathways to regulate gene expression and participates in a wide variety of physiological processes including skeletal muscle differentiation and regeneration, cardiac hypertrophy, and neuronal signaling.[2−6] CN is a heterodimeric protein complex comprised of a ∼60 kDa catalytic subunit, CNA, and a ∼19 kDa regulatory subunit, CNB. As shown in Figure 1, there are four well-established domains in CNA: (i) a catalytic domain (14_A-342_A, where the number and subscript letter indicate the residue number and the corresponding subunit (i.e., CNA), respectively), (ii) a CNB binding domain (343_A-373_A), (iii) a CaM interaction region (390_A-414_A), and (iv) an autoinhibitory (AI) motif (469_A-486_A).[1,7] In addition, a section of the unstructured region within the CNA subunit that is important for stabilizing the interactions within CNA upon calmodulin binding has recently been identified.[8−10] The CN active site, which is located in the catalytic domain, contains a binuclear metal center that is critical for phosphatase activity. The two metals have been identified as Zn, which is coordinated with Asn_{150A}, His_{199A}, and His_{281A}, (the subscript number and letter indicate the residue number and the CN subunit, respectively), and Fe, which is coordinated with Asp_{90A} and His_{92A}.[1,7,11−13] The existence of both Fe^{3+}-Zn^{2+}[11,12,14,15] and Fe^{2+}-Zn^{2+}[16,17] forms have been reported, and the oxidation states of Fe in the active enzyme remain inconclusive. The CNB subunit is a CaM-like protein possessing four EF-Hand Ca^{2+} binding domains.[18] The Ca^{2+} binding regions I (31_B-42_B) and II (63_B-74_B), located close to the N-terminus, have relatively low Ca^{2+} affinity,[19−21] whereas Ca^{2+} binding regions III (100_B-111_B) and IV (141_B-152_B), located close to the C-terminus, have relatively high affinity and are occupied even in unstimulated cells where the Ca^{2+} concentration is lower than 10^{-7} M. Under normal conditions, the binuclear metal active site located in the groove of the CNA catalytic domain is blocked by AI and the enzyme is inactive. Upon an increase in Ca^{2+} concentration during extracellular stimulation, CaM activation caused by Ca^{2+} binding enables its interaction with

Received: August 5, 2014
Revised: October 5, 2014
Published: October 6, 2014

CN subunit A (CNA): ~60 kDa

*MSEPKAIDPKLST*TDRVVKAVPFPPSHRLTAKEVFDNDGKPRVDILKAHLM$_{51}$KEGRLEESVALRIITEGASILRQEKNLL
DIDAPVTVCGDIHGQFFDLM$_{99}$KLFEVGGSPANTRYLFLGDYVDRGYFSIECVLYLWALKILYPKTLFLLRGNHECRHLTEYF
TFKQECKIKYSERVYDACM$_{179}$DAFDCLPLAALM$_{191}$NQQFLCVHGGLSPEINTLDDIRKLDRFKEPPAYGPM$_{227}$CD
ILWSDPLEDFGNEKTQEHFTHNTVRGCSYFYSYPAVCEFLQHNNLLSILRAHEAQDAGYRM$_{290}$YRKSQTTGFPSLITIFSA
PNYLDVYNNKAAVLKYENNVM$_{329}$NIRQFNCSPHPYWLPNFM$_{347}$DVFTWSLPFVGEKVTEM$_{364}$LVNVLNICS*DD*
ELGSEEDGFDGATAAARKEVIRNKIRAIGKM$_{406}$ARVFSVLREEESESVLTLKGLTPTGM$_{431}$LPSGVLSGGKQTLQSATVE
*AIEADEAIKGFSPQHKIT*SFEEAKGLDRINERM$_{483}$PPR*RDA*M$_{490}$*PSDANLNSINKALTSETNGTDSNGSNSSNIQ*

CN subunit B (CNB): ~19 kDa

MGNEASYPLEM$_{11}$CSHFDADEIKRLGKRFKKLDLDNSGSLSVEEFM$_{44}$SLPELQQNPLVQRVIDIFDTDGNGEVDFKEF
IEGVSQFSVKGDKEQKLRFAFRIYDM$_{101}$DKDGYISNGELFQVLKM$_{118}$M$_{119}$VGNNLKDTQLQQIVDKTIINADKD
GDGRISFEEFCAVVGGLDIHKKM$_{166}$VVDV

Figure 1. Amino acid sequences and protein domains of CNA and CNB. Met residues are bolded and numbered, Lys residues are shown in larger font size. For the CNA subunit (UnitProt entry Q08209), the catalytic domain is color coded in purple, the CNB binding motif is in red, the CaM interaction domain is in green, and the autoinhibitory region is in orange. For the CNB subunit (UnitProt entry P63098), the EF-hands are color coded in blue, and the corresponding Ca^{2+}-binding pockets are color coded in cyan. Regions of the protein sequences not visible in the crystal structure (PDB entry 1AUI)[7] are in italic text.

the CaM binding domain in CNA and removes the AI domain from the catalytic site, resulting in CN activation. Moreover, Ca^{2+} occupancy of the two N-terminal low-affinity sites causes a conformational change in the tightly associated CNA and facilitates the binding of CNA with CaM.[19]

CN is reported to be inactivated by H_2O_2- or superoxide-induced oxidation both *in vivo* and *in vitro*.[22−26] Several mechanisms for this inactivation have been proposed. One mechanism postulated that the redox regulation of CN is induced by the formation of a disulfide bridge between two vicinal cysteine residues in the catalytic region of CNA.[15] However, how the bridging affects CN enzymatic activity remains unclear as the only pair of conserved cysteine residues (Cys_{228A} and Cys_{256A}) which could form the disulfide bond are not close to the active binuclear metal center.[7,13] A bridging-induced conformational change in the catalytic domain of CNA was proposed as the cause of inactivation; however, this hypothesis has not been demonstrated experimentally. Another proposal suggested that the binuclear active site exists as Fe^{2+}-Zn^{2+} and that CN inactivation is caused by oxidation of Fe^{2+} to Fe^{3+}.[17] However, this finding is in conflict with many previous studies demonstrating Fe^{3+}-Zn^{2+} as the form with maximum activity.[12,14,15] Previously, Carruthers et al. reported that Met_{406A}, located in the CaM binding motif of CNA, was highly susceptible to oxidation, resulting in a shift in Ca^{2+}-dependence and a decrease in CaM/CN binding affinity, suggesting that oxidative inactivation of CN is caused by direct inhibition of the CN-CaM interaction.[27] However, it was found that oxidation of a CN mutant lacking Met_{406A} (i.e., $M_{406A}L$) also showed reduced activity, indicating that oxidation of Met_{406A} was not solely responsible for the observed oxidation-induced CN inactivation. For example, global or local conformational changes associated with the oxidation of methionine residues located within structurally important regions of the CN complex, such as the Ca^{2+} binding domains, could also play a critical role in the oxidative inactivation process. However, this hypothesis has not been examined to date.

Mass spectrometry, in conjunction with selective covalent labeling of accessible amino acid side functional groups, can be used to provide structural information (albeit relatively low resolution) about changes in protein surfaces and conformations occurring as a result of protein folding or unfolding, protein−protein interactions, protein−ligand binding, or protein modification.[28−30] However, identification and characterization of the often low abundance modified peptides within a complex mixture of largely unmodified peptides that is typically generated following proteolytic digestion of a large protein or protein complex, and quantification of the modification site occupancies (i.e., the determinant of accessibility at a specific residue), present a significant analytical challenge. Previously, we reported the development of a strategy for mapping solvent-accessible lysine residues within proteins, via covalent labeling with a novel amine-specific protein modification reagent, *S*,*S*′-dimethylthiobutanoylhydroxysuccinimide ester (DMBNHS), and its application to a model protein, namely, human cellular retinoic acid binding protein II.[31] After reaction at different reagent to protein ratios, followed by protein digestion, capillary HPLC-ESI-MS and automated collision-induced dissociation−tandem mass spectrometry (CID-MS/MS) in an ion trap mass spectrometer, the modified peptides, and the number of modifications within each peptide, were readily identified via the dominant characteristic neutral loss(es) of a dimethylsulfide moiety from the modified lysine amino acid side chain.[31,32] The observation of the neutral losses were then used to automatically trigger the acquisition of a "data-dependent neutral loss mode" MS^3 spectrum for peptide sequence and modification site(s) characterization. Using this approach, the experimentally determined relative accessibilities of the various lysine residues within CRABP II were found to show good agreement with those calculated from the known solution structure.[31]

Here, the relative susceptibility of CN methionine residues toward H_2O_2-induced oxidation was first determined using a multienzyme digestion strategy coupled with capillary HPLC-ESI-MS and -MS/MS. Then, the DMBNHS chemical labeling and tandem mass spectrometry analysis strategy described above was applied to map changes in the accessibility of lysine residues between native and oxidized forms of CN, to identify regions within the protein complex that undergo significant conformational perturbation upon oxidative modification and therefore may be involved in the mechanism(s) responsible for oxidation-induced CN inactivation.

EXPERIMENTAL SECTION

Materials. All chemicals were of analytical reagent (AR) grade. Ethylene glycol-bis(2-aminoethyl ether)-*N*,*N*,*N*′,*N*′-tetraacetic acid (EGTA), dithiothreitol (DTT), iodoacetamide, bovine catalase, tris(hydroxymethyl)aminomethane hydrochloride (Tris·HCl), tris(hydroxymethyl)aminomethane (Tris·base), and HEPES were purchased from Sigma-Aldrich (St. Louis, MO, USA). KCl, $MgCl_2$, $CaCl_2$, and H_2O_2 (30% solution) were purchased from Columbus Chemical Industries (Columbus, WI, USA). Dimethylformamide (DMF) was from Jade Scientific (Canton, MI, USA). Glacial acetic acid and water (HPLC grade) were from Mallinckrodt Chemicals (Phillipsburg, NJ, USA). Acetonitrile (HPLC grade) and iodomethane were purchased from EMD Chemicals (San Diego, CA, USA). Sodium hydroxide (NaOH) and formic acid were from Spectrum Chemical Mfg. (Gardena, CA, USA). Trifluoroacetic acid (TFA) was purchased from Pierce (Rockford, IL, USA). Mass spectrometry grade Glu-C was purchased from Thermo Fisher Scientific (Waltham, MA, USA). Sequencing grade

dx.doi.org/10.1021/bi5009744 | *Biochemistry* 2014, 53, 6754−6765

modified trypsin was from Promega (Madison, WI, USA). Sequencing grade Lys-C was obtained from Roche Diagnostics (Indianapolis, IN, USA). Human calcineurin was prepared as previously described.[27] DMBNHS was prepared via a three-step process as described previously.[31]

Protein Oxidation. Ten microliters of 250 mM H_2O_2 was added (final H_2O_2 concentration: 12 mM) to 200 μL aliquots of 0.40 μg/μL CN in 10 mM HEPES buffer (pH 7.6) (10 mM HEPES, 100 mM KCl, 1 mM $MgCl_2$) and 0.1 mM $CaCl_2$. Oxidation was allowed to occur at room temperature in the dark for 15, 30, 45, 60, 120, and 240 min, and then 40 μL of catalase in 10 mM HEPES buffer (pH 7.6) was added and the reaction was quenched at room temperature for 5 min. After oxidation, each aliquot was divided into nine samples and then stored at −80 °C until further use. A control native CN sample (i.e., time 0) was also prepared by adding 50 μL of 10 mM HEPES buffer (pH 7.6) to 200 μL of 0.40 μg/μL CN solution in 10 mM HEPES buffer (pH 7.6).

DMBNHS Protein Modification. Six aliquots of each CN sample (i.e., 0, 15, 30, 45, 60, 120, and 240 min time points) were modified by the addition of 1 μL of DMBNHS solution dissolved in 25%DMF/75%H_2O (prepared immediately before use) at concentrations of 0.0, 0.5, 1.0, 2.0, 5.0, and 10.0 mM. After incubation for 30 min at room temperature, the reaction was quenched by the addition of 8 μL of Tris (pH 8.3) at a 160-fold molar excess over DMBNHS and then stored at −80 °C until further use.

Protein Digestion. Each of the CN samples described above were diluted with 10 mM HEPES buffer (pH 7.6) to a final volume of 44 μL followed by addition of 8 μL of 10 mM EGTA. Reduction and alkylation of CN disulfide bonds were then performed by the addition of 2 μL of 0.1 M DTT and incubation at 60 °C for 30 min, followed by the addition of 2 μL of 0.25 M iodoacetamide and further reaction at room temperature for 1 h in the dark. Two microliters of 0.1 M DTT was then added to inactivate excess iodoacetamide at room temperature for 30 min and diluted with 10 mM HEPES buffer (pH 7.6) to a final volume of 70 μL. The three aliquots of each of the CN samples at 0, 15, 30, 45, 60, 120, and 240 min H_2O_2 oxidation time points were then digested separately with Glu-C, trypsin, and Lys-C, while the DMBNHS-modified CN samples were digested only with Glu-C. For digestion using Glu-C, the pH of the CN samples was adjusted to 8.0 with 0.2 M NaOH followed by addition of 4 μL of 0.1 μg/μL Glu-C in H_2O. The digestion was performed at 30 °C for 16 h. For trypsin digestion, the pH of the CN samples was adjusted to 7.8 with 0.2 M NaOH followed by addition of 4 μL of 0.2 μg/μL trypsin in H_2O, and then the reaction mixture was incubated at 37 °C for 16 h. For Lys-C digestion, the pH of the CN sample was brought up to 8.0 with 0.2 M NaOH followed by addition of 4 μL of 0.2 μg/μL Lys-C in H_2O and digestion for 16 h at 37 °C. Finally, 0.5 μL of formic acid was added to inactivate the proteases, and then the samples were stored at −20 °C until further analysis.

Mass Spectrometry Analysis. HPLC-ESI-MS followed by data-dependent CID and/or electron transfer dissociation (ETD)-MS/MS analysis of the digests from oxidized CN samples, and HPLC-ESI-MS followed by data-dependent constant neutral loss (DDCNL) CID-MS/MS, -MS^3, or targeted ETD-MS/MS analysis of the digests from DMBNHS-modified CN samples, were performed using a Thermo Fisher Scientific LTQ Orbitrap Velos mass spectrometer (Thermo, San Jose, CA, USA) coupled with an Advance nESI source and Paradigm MS4 capillary RP-HPLC system (Michrom Bioresources, Auburn, CA, USA). Analyses were performed using automated methods created by the Xcalibur software (Thermo, San Jose, CA, USA). Five microliters of each sample (0.20 pmol/μL for digests of native or oxidized CN samples, and 0.35 pmol/μL for digests of native or oxidized DMBNHS-modified CN samples) in 3% acetic acid/5% acetonitrile was loaded from a Paradigm AS1 autosampler (Michrom Bioresources, Auburn, CA, USA) onto a peptide CapTrap (Michrom Bioresources, Auburn, CA, USA) at a flow rate of 15 μL/min using 0.1% trifluoroacetic acid/2% acetonitrile as the loading buffer. After 5 min loading time, the peptides concentrated on the peptide CapTrap were eluted onto a 200 μm id × 50 mm fused silica column packed with Magic C18AQ (3 μm) (Michrom Bioresources, Auburn, CA, USA) at a flow rate of 2 μL/min using a linear 45 min (for digests from native or oxidized CN samples) or 70 min (for digests from native or oxidized DMBNHS-modified CN samples) gradient from 95% solvent A (0.1% formic acid in H_2O) to 50% solvent B (0.1% formic acid in CH_3CN).

The ion transfer tube of the mass spectrometer was set at 250 °C, and the spray voltage was maintained at 1.4 kV. The S-lens was set at 57%. Full MS scans were acquired from m/z 300−2000 in the Orbitrap mass analyzer at a mass resolving power of 60 000. Full scans were taken at an AGC target value of 2.0×10^5, with a 10 ms maximum injection time in the ion trap. All spectra were recorded in centroid mode. The isolation window was maintained at 2.0 m/z for all MS/MS and MS^3 analysis. During CID-MS/MS and -MS^3, using an AGC target value of 1.0×10^4 and a 100 ms maximum injection time in the ion trap, isolated precursor ions were fragmented with a normalized collision energy of 35% with an activation time of 10 ms and an activation q value of 0.25. For ETD-MS/MS, the AGC target value and maximum injection time was the same as the CID-MS/MS experiments, while the AGC target value and maximum injection time of the fluoranthene reagent anion were set at 2.0×10^4 and 100 ms, respectively. ETD was carried out with supplemental activation enabled, at a normalized energy of 15%. The activation time was optimized between 60 ms and 100 ms for the 2+ charge state and proportionally scaled down for higher charge states (e.g., if a 60 ms reaction time was used for a 2+ charge state, a 40 ms reaction time was used for the 3+ charge state, a 30 ms reaction time was used for a 4+ charge state, etc.). Except for targeted ETD-MS/MS analysis, dynamic exclusion was enabled to acquire three MS/MS or MS^3 scans on a given precursor ion within 30 s, prior to dynamic exclusion for 10 s.

For both CID- and ETD-MS/MS analysis of the digests from oxidized CN, the mass spectrometer was programmed to operate in a data-dependent mode, where each survey MS scan was followed by MS/MS of the five most intense ions (signal threshold was set at 1.0×10^4 counts). For CID-MS/MS and -MS^3 analysis of the digests from native or oxidized DMBNHS-modified CN, the mass spectrometer was operated in a DDCNL mode by performing CID-MS/MS scans on the five most intense ions from each MS survey scan, while simultaneously searching for defined neutral losses (within an m/z variance of ±0.5) corresponding to single, double, and triple $S(CH_3)_2$ neutral losses from $[M^{N+} + (m\text{-}N)H]^{m+}$ precursor ions, where M represents the peptide, N represents the number of modifications, and m represents different charge states ranging from +2 to +5 (see Supplemental Table S1,

dx.doi.org/10.1021/bi5009744 | Biochemistry 2014, 53, 6754−6765

Table 1. Summary of Observed Methionine Residues from Proteolytic Digests of CN, Their Predicted Solvent Accessibilities and Observed Pseudo-First-Order Oxidation Rate Constants (k_{ox})

	peptides observed from the corresponding digests					
methionine residue	trypsin digest	Glu-C digest	Lys-C digest	Lys-C digest from Carruthers et al.[a]	predicted solvent accessibilities[b]	calculated pseudo-first-order oxidation rate constants (k_{ox}) s^{-1}
Met_{51A}[c]		34_A-53_A			38.6%	1.4×10^{-5}
Met_{99A}	77_A-100_A			77_A-100_A	6.6%	3.0×10^{-6}
Met_{227A}	218_A-243_A and 220_A-243_A		220_A-243_A	220_A-243_A	2.8%	3.1×10^{-6}
Met_{329A}	324_A-332_A				4.1%	6.7×10^{-6}
Met_{364A}	361_A-392_A	364_A-394_A	361_A-393_A		0.4%	1.5×10^{-6}
Met_{406A}		395_A-416_A	406_A-424_A	406_A-424_A	N/A[d]	3.1×10^{-5}
Met_{431A}	425_A-441_A	419_A-450_A	425_A-441_A	425_A-441_A	N/A	8.4×10^{-5}
$Met_{483A,490A}$		482_A-506_A	475_A-501_A	475_A-501_A	17.5% (Met_{483A})	5.6×10^{-5} (Met_{483A})
					N/A (Met_{490A})	8.4×10^{-5} (Met_{490A})
Met_{490A}	488_A-501_A				N/A	8.4×10^{-5}
Met_{11B}		11_B-19_B		2_B-21_B	12.3%	2.1×10^{-6}
Met_{44B}	30_B-57_B	43_B-48_B		29_B-73_B	43.8%	6.8×10^{-5}
Met_{101B}	98_B-117_B	90_B-111_B	92_B-103_B	92_B-103_B	26.7%	1.5×10^{-5}
$Met_{118B,119B}$			118_B-125_B		30.8% (Met_{118B})	1.2×10^{-5} (Met_{118B})
					3.9% (Met_{119B})	1.6×10^{-6} (Met_{119B})
Met_{166B}	166_B-170_B	153_B-170_B	166_B-170_B		0.3%	9.3×10^{-5}

[a]Data obtained from ref 27. [b]Solvent accessibilities were predicted based on the CN crystal structure from PDB entry 1AUI,[7] using the GetArea program.[33] [c]The subscript number and letter indicate the residue number and the corresponding CN subunit, respectively. [d]N/A; predicted solvent accessibilities could not be determined as these residues are not observed in the CN crystal structure.

Supporting Information).[31] If a predefined neutral loss was detected above a threshold abundance of 1.0×10^4 counts, CID-MS^3 was automatically initiated to isolate then further dissociate the most intense neutral loss product ion. For targeted ETD-MS/MS analysis of digests from native or oxidized DMBNHS-modified CN, the mass spectrometer was operated in a data-dependent mode where only predefined precursor ions of interest observed within a ± 0.5 min elution window determined from previous HPLC-ESI-MS, CID-MS/MS, and -MS^3 experiments, were selected for dissociation. Characterization of the peptide sequences and the oxidation or DMBNHS modification sites were determined by manual interpretation of the MS/MS or MS^3 spectra. The program GetArea[33] was used, with all parameters set at default values, to calculate the solvent accessibilities of lysine amino acid side chains of CN, based on the reported CN crystal structure.[7]

Data Analysis. Unless indicated otherwise, the relative abundances of peptide ions were determined from the MS spectra averaged over the corresponding chromatographic peaks. If multiple charge states for a precursor ion were observed, then the abundance was calculated by combining the abundance from all charge states. For peptides with only one modifiable residue (i.e., either methionine or lysine), the percent unmodified residue remaining after each reaction condition was calculated using eq 1,

$$MS_{(unmodified)}/(MS_{(unmodified)} + MS_{(modified)}) \times 100\% \quad (1)$$

where $MS_{(unmodified)}$ indicates the MS ion abundance of the unmodified peptide and $MS_{(modified)}$ indicates the MS ion abundance of the modified peptide. For peptides with multiple modifiable residues and whose isomeric-modified forms were resolved chromatographically, the percent unmodified form of each residue remaining after each reaction condition was determined by eq 2,

$$(MS_{(unmodified)} + \sum MS_{(pUnmodified)})/(MS_{(unmodified)} + \sum MS_{(modified)}) \times 100\% \quad (2)$$

where $MS_{(pUnmodified)}$ indicates the MS ion abundance of a partially modified peptide isomer where the residue under investigation was unmodified. For peptides with multiple modifiable residues and whose isomeric-modified forms coeluted during HPLC separation (this was only observed in the case of some DMBNHS-modified peptides), the abundance of the partially modified peptide isomers with different site(s) of modification could not be determined solely from the MS ion abundance. Therefore, the percent unmodified form of each residue remaining after each reaction condition was determined by eq 3,

$$(MS_{(unmodified)} + \sum MS_{(pModified)} \times (\sum MS/MS_{(pUnmodified)}/(\sum MS/MS_{(modified)}))/(MS_{(unmodified)} + \sum MS_{(modified)} \times 100\% \quad (3)$$

where $MS_{(pModified)}$ indicates the MS ion abundance of partially modified peptide isomers, $\sum MS/MS_{(pUnmodified)}$ is the summed abundances of the characteristic ETD-MS/MS product ions from a particular modified peptide isomer where the residue under investigation was unmodified, and $\sum MS/MS_{(pModified)}$ is the summed abundance of the characteristic ETD-MS/MS product ion abundances from all modified peptide isomers.

For the methionine oxidation study, the results from triplicate HPLC-ESI-MS analysis for each reaction were then averaged and used for the determination of pseudo-first-order methionine oxidation rate constants (k_{ox}), as described by Carruthers et al.,[27] where k_{ox} was determined from the plots of average percent native methionine residue versus oxidation time (t_{ox}) as ln(native methionine residue%) = $-k_{ox}t_{ox}$. If a methionine residue was observed in multiple digests, the reported oxidation rate constant was obtained by averaging the

dx.doi.org/10.1021/bi5009744 | Biochemistry 2014, 53, 6754−6765

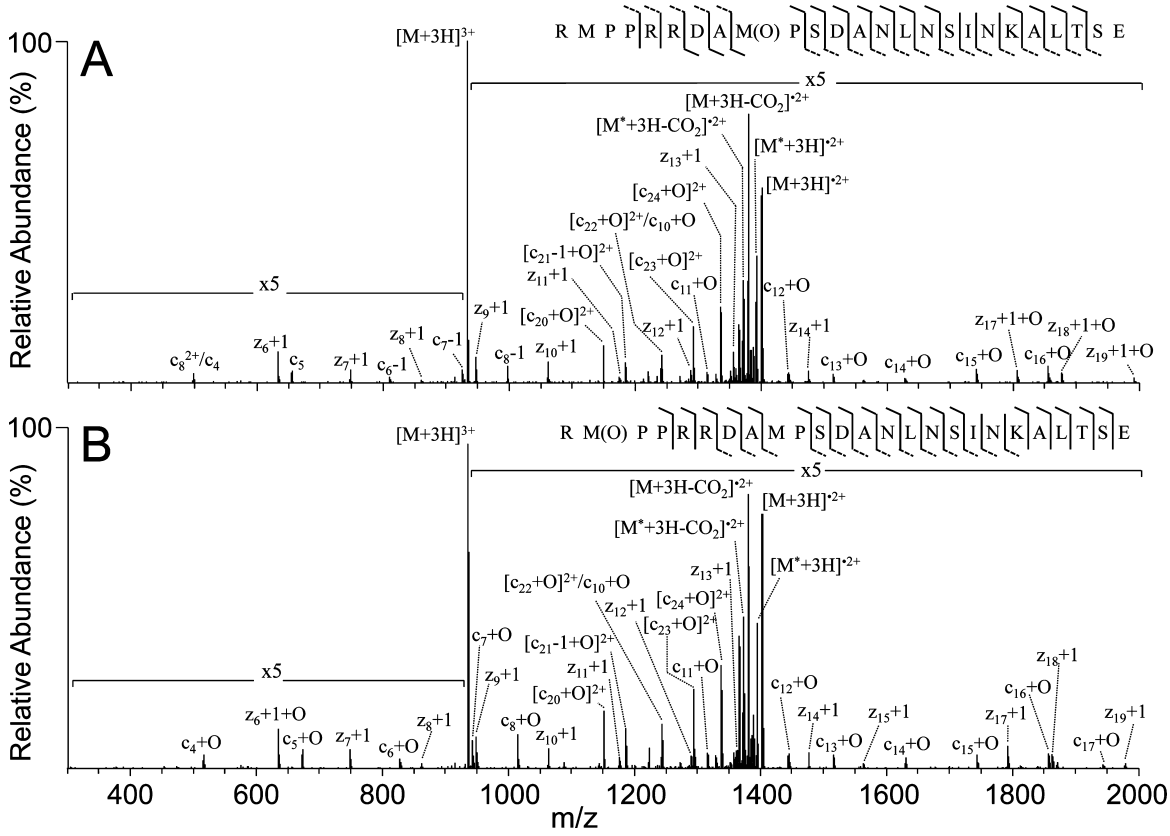

Figure 2. Ion trap ETD-MS/MS characterization of the triply protonated precursor ion isomers of singly oxidized CNA peptide 482_A-506_A containing (A) oxidized Met_{490A} and (B) oxidized Met_{483A}. A "+O" indicates a sequence ion containing one oxidation site. A superscript * indicates the loss of NH_3. A dashed line in the sequence indicates an unoxidized sequence ion was observed, while a solid line indicates that a singly oxidized sequence ion was observed.

results from the peptides observed in each digest. For the lysine DMBNHS labeling experiments, the results from triplicate HPLC-ESI-MS and/or ETD-MS/MS analysis were averaged and used for the determination of second-order DMBNHS modification rate constants (k_{DMBNHS}). k_{DMBNHS} was determined as $\ln(\text{unmodified lysine residue}\%) = -k_{DMBNHS}(\text{DMBNHS/CN})t_{DMBNHS}$ from the plots of average percent unmodified lysine residues versus molar reaction ratio of DMBNHS over CN. t_{DMBNHS} was a fixed value at 1800 s.

RESULTS AND DISCUSSION

Quantification of the Susceptibility of Methionine Residues toward Oxidation. To determine the sensitivity of methionine residues within CN toward oxidation by H_2O_2, CN was incubated with 12 mM H_2O_2 for 0, 15, 30, 45, 60, 120, and 240 min, digested with Lys-C, trypsin, or Glu-C, then analyzed in triplicate by capillary HPLC-ESI-MS. The peptides were identified by their monoisotopic m/z values obtained from the high resolution/accurate mass spectra and confirmed by CID- and/or ETD-MS/MS analysis in the ion trap. Fifteen of the total 19 methionine residues were observed. The observed methionine residues from the corresponding peptides in the three different digests, compared to the results reported by Carruthers et al.,[27] along with the predicted solvent accessibilities based on the CN crystal structure,[7] are listed in Table 1. Note that some of the peptides observed here from the Lys-C digest are different than those observed by Carruthers et al. (i.e., some peptides observed by Carruthers et al. were not observed here, and vice versa).[27] This is likely attributed to differences in the chromatographic separation conditions used in each study.

It can be seen from Table 1 that some peptides contain two methionine residues. For example, CNA subunit peptides 482_A-506_A from the Glu-C digest and 475_A-501_A from the Lys-C digest both contain Met_{483A} and Met_{490A}, while CNB subunit peptide 118_B-125_B from the Lys-C digest contains both Met_{118B} and Met_{119B}. Thus, two isomeric forms will exist for the singly oxidized forms of these peptides. Fortunately, the pairs of singly oxidized isomers for each of these peptides were chromatographically resolved, and their oxidation sites were determined by CID- or ETD-MS/MS, thereby allowing the oxidation rate constant for each methionine residue to be determined. For example, Figure 2A shows the ETD-MS/MS spectrum of peptide 482_A-506_A from the Glu-C digest, oxidized at Met_{490A}, while Figure 2B shows the ETD-MS/MS spectrum of the same peptide, oxidized at Met_{483A}. In Figure 2A, the presence of nonoxidized sequence ions c_5, c_6-1, c_7-1, c_8-1, z_6+1, z_7+1, z_8+1, z_9+1, z_{10}+1, z_{11}+1, z_{12}+1, z_{13}+1, and z_{14}+1, and oxidized sequence ions c_{10}+O, c_{11}+O, c_{12}+O, c_{13}+O, c_{14}+O, c_{15}+O, c_{16}+O, $[c_{20}+O]^{2+}$, $[c_{21}+O]^{2+}$, $[c_{22}+O]^{2+}$, $[c_{23}+O]^{2+}$, z_{15}+O, z_{17}+O+1, z_{18}+O+1, and z_{19}+O+1 readily allowed localization of the oxidation site to Met_{490A}. Similarly, the oxidation site in Figure 2B was readily localized to Met_{483A}.

Notably, more complete sequence coverage was obtained by using ETD compared to CID for these peptides (see Supplemental Figure S1A,B, Supporting Information). The lower, but complementary, sequence coverage obtained by CID-MS/MS was attributed as being due to the facile loss of

dx.doi.org/10.1021/bi5009744 | Biochemistry 2014, 53, 6754−6765

methane sulfenic acid (CH_3SOH), which occurs as a dominant process under conditions of low proton mobility (the +3 precursor ion of the 482_A-506_A peptide observed here corresponds to a "nonmobile" protonation state).[34] In contrast, due to the radical-driven cleavage mechanism of ETD, the neutral loss of sulfenic acid is not observed.[35] The oxidation sites for the isomers of the singly oxidized 475_A-501_A and 118_B-125_B peptides were also identified by ETD- and CID-MS/MS (data not shown). Therefore, the oxidation rates of all observed methionine residues could be individually quantified.

The fraction of each of the observed methionine residues within the CN protein complex remaining in its nonoxidized state were then plotted against oxidation time to calculate the corresponding pseudo-first-order oxidation rate constants (k_{ox}). Two examples are shown in Figure 3 for the tryptic peptides

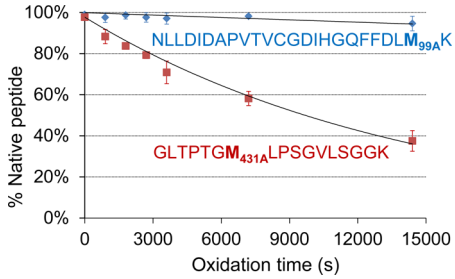

Figure 3. Percentage of methionine-containing CN peptides remaining in the reduced form following treatment with 12 mM H_2O_2 for 0, 15, 30, 45, 60, 120, and 240 min. Data points from the Met_{99A}-containing tryptic peptide (77_A-100_A), NLLDIDAPVTVCGD-IHGQFFDL**M**$_{99A}$K, are indicated with a ♦. Data points from the Met_{431A}-containing tryptic peptide (425_A-441_A), GLTPTG**M**$_{431A}$L-PSGVLSGGK, are indicated with a ■. All data were run in triplicate and fitted with a single exponential. Error bars are shown as ± standard deviation.

77_A-100_A (Met_{99A}) and 425_A-441_A (Met_{431A}). Met_{431A} exhibited a higher susceptibility toward oxidation compared to Met_{99A}, with calculated k_{ox} values of 8.4×10^{-5} s^{-1} and 3.0×10^{-6} s^{-1}, respectively. Similar plots for each of the observed methionine residues from each digest are shown in Supplemental Figure S2, Supporting Information. From each of these plots, pseudo-first-order reaction rate constants were calculated and are shown in Figure 4, as solid labels. The rate constants determined by Carruthers et al.[27] are also included in Figure 4 for comparison, represented by open labels. On the basis of these results, methionine residues above an arbitrary threshold of $k_{ox} > 2.0 \times 10^{-5}$ s^{-1} were considered as being particularly susceptible to oxidation.

It can be seen from Supplemental Figure S2, Supporting Information that when the same methionine residue was observed in different digests, they generally underwent similar extents of oxidation as a function of H_2O_2 incubation times. The Lys-C digests showed a slightly higher extent of oxidation, which may have resulted from a small variance in H_2O_2 concentration during the sample preparation process for this particular digest. Nonetheless, the calculated oxidation rate constants were consistent among the different digests, as evidenced by the error bars in Figure 4 that show the standard deviations when the same methionine residue was observed in peptides from different digests.

The results obtained using the multienzyme digestion strategy described here were generally consistent with those

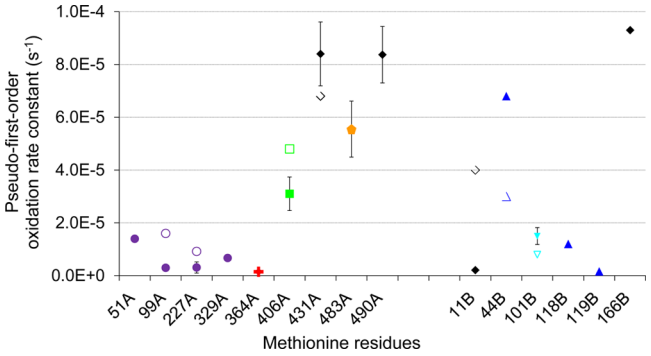

Figure 4. Pseudo-first-order oxidation rate constants determined for each observed CN methionine residue located in the catalytic domain (purple solid circle), CNB binding domain (red plus sign), CaM binding domain (green solid box) and autoinhibitory region (orange solid pentagon) of CNA, the CNA binding region (blue solid up triangle) and Ca^{2+} binding domain (light blue solid down triangle) of CNB, and the nonfunctional regions (♦) of CNA and CNB. Open labels indicate the data reported by Carruthers et al.[27] When the same methionine residue was observed within peptides from different digests, the data are reported as the average, with error bars shown as ± standard deviation.

previously reported by Carruthers et al., except for Met_{11B} and Met_{44B}. These differences might be due to the variations in conformation between these two batches of proteins. However, the results obtained in the current study are quite consistent with the predicted solvent accessibility (SA) for Met_{11B} of 12.3% and for Met_{44B} of 43.8% (calculated from the crystal structure of human CN with a free N-terminus). Furthermore, the N-terminus of the CNB subunit within the CN complex examined here was myristoylated, and the crystal structure of a bovine CN protein complex with N-terminal myristoylation of CNB shows that the extended myristoyl group is laid over the 1_B-12_B residues.[13] Therefore, the actual SA of Met_{11B} is expected to be lower than 12.3%, which supports the low oxidation rate constant determined for this residue. Generally, the relative susceptibilities of observed methionine residues determined here show good correlation with the calculated solvent accessibility based on the known crystal structure.[7] However, it should be noted that Met_{483A} and Met_{166B} have relatively low calculated solvent accessibility but showed high sensitivity toward oxidation. These differences might be a reflection of the different conformations proteins adopt in the dynamic (i.e., solution) versus static (i.e., crystal) states, as both Met_{483A} (located in the linker region between the CaM binding and autoinhibitory domain) and Met_{166B} (located on CNB C-terminal) reside in flexible regions of the protein based on the crystal structure.

The oxidation rate constants determined here are expected to be dependent upon the native structure of CN. However, conformational changes resulting from sequential secondary oxidation of the oxidized CN (discussed later), may also occur. To surmise to what extent the protein may undergo secondary oxidation, the probability of a protein being singly oxidized ($P(1\ ox)$) and doubly oxidized ($P(2\ ox)$) upon being oxidized for 15 min were calculated using eqs 4 and 5, respectively.

$$P(1\ ox) = \sum_{i=1}^{19} p_i \left(\prod_{j=1, j\neq i}^{19} (1 - p_j) \right) \quad (4)$$

dx.doi.org/10.1021/bi5009744 | Biochemistry 2014, 53, 6754−6765

Table 2. Summary of DMBNHS Modification Rate Constants Determined for Lysine Residues from Glu-C Digests of Native and 15 min Oxidized CN

lysine residue	peptide	predicted solvent accessibilities[a]	oxidation time (min)	calculated second-order DMBNHS reaction rate constants k_{DMBNHS} ($M^{-1}s^{-1}$)
Lys_{40A}[b]	34_A-44_A	69.00%	0	1.0×10^{-7}
			15	1.5×10^{-6}
Lys_{40A}	34_A-53_A	69.00%	0	5.0×10^{-7}
			15	8.3×10^{-6}
Lys_{47A}		45.30%	0	1.2×10^{-6}
			15	1.8×10^{-6}
Lys_{52A}		64.20%	0	1.2×10^{-6}
			15	1.8×10^{-6}
Lys_{393A}	364_A-394_A	N/A[d]	0	1.3×10^{-6}
			15	2.3×10^{-6}
	373_A-394_A	N/A	0	1.2×10^{-6}
			15	2.0×10^{-6}
Lys_{399A}	395_A-416_A	N/A	0	4.0×10^{-7}
			15	1.1×10^{-6}
Lys_{405A}		N/A	0	6.3×10^{-7}
			15	1.3×10^{-6}
$Lys_{424A,441A}$	419_A-450_A	N/A	0	1.6×10^{-6}
			15	2.6×10^{-6}
Lys_{424A}[c]	419_A-450_A	N/A	0	3.2×10^{-7}
			15	1.2×10^{-6}
Lys_{441A}[c]		N/A	0	1.0×10^{-7}
			15	1.6×10^{-7}
Lys_{459A}	451_A-472_A	N/A	0	8.9×10^{-7}
			15	1.3×10^{-6}
	457_A-472_A	N/A	0	1.4×10^{-6}
			15	2.2×10^{-6}
Lys_{466A}	451_A-472_A	N/A	0	1.4×10^{-6}
			15	2.3×10^{-6}
	457_A-472_A	N/A	0	1.7×10^{-6}
			15	2.6×10^{-6}
Lys_{474A}	473_A-481_A	51.90%	0	7.2×10^{-7}
			15	1.9×10^{-6}
Lys_{501A}	482_A-506_A	N/A	0	1.9×10^{-6}
			15	3.3×10^{-6}
$Lys_{21B,25B,28B,29B}$	20_B-42_B	83.4% (Lys_{21B})	0	2.9×10^{-6}
		70.1% (Lys_{25B})		
		85.2% (Lys_{28B})		
		58.5% (Lys_{29B})		
			15	5.0×10^{-6}
Lys_{21B}[c]	20_B-42_B	83.40%	0	1.7×10^{-6}
			15	2.7×10^{-6}
Lys_{73B}	70_B-77_B	37.20%	0	4.9×10^{-7}
			15	1.1×10^{-6}
Lys_{85B}	75_B-89_B	68.50%	0	1.8×10^{-6}
			15	2.7×10^{-6}
Lys_{88B}		54.50%	0	2.2×10^{-6}
			15	3.5×10^{-6}
$Lys_{9B,103B}$	90_B-111_B	3.8% (Lys_{91B})	0	3.8×10^{-7}
		49.8% (Lys_{103B})	15	1.4×10^{-6}
Lys_{91B}[c]	90_B-111_B	3.80%	0	3.2×10^{-7}
			15	1.2×10^{-6}
Lys_{103B}[c]		49.80%	0	1.0×10^{-7}
			15	1.6×10^{-7}
Lys_{164B}	153_B-170_B	75%	0	1.2×10^{-6}
			15	2.3×10^{-6}
Lys_{165B}		61%	0	1.3×10^{-6}
			15	2.3×10^{-6}

[a]Solvent accessibilities were predicted based on the CN crystal structure from PDB entry 1AUI,[7] using the GetArea program.[33] [b]The subscript number and letter indicate the residue number and the corresponding CN subunit, respectively. [c]Calculation of k_{DMBNHS} of these residues were based on the relative intensities of ETD-MS/MS product ions. [d]N/A; Predicted solvent accessibilities could not be determined as these residues are not observed in the CN crystal structure.

$$P(2\ \mathrm{ox}) = \{\sum_{i=1}^{19} p_{i1} \cdot p_{i2} \left(\prod_{j=1, j\neq i1, j\neq i2}^{19} (1 - p_j) \right)\}/2! \quad (5)$$

In these equations, $p_{i,j}$ is the probability of a specific methionine residue being oxidized at the 15 min oxidation time point, determined from the data in Supplemental Figure S2, Supporting Information. Four methionine residues located in the catalytic domain were not observed, and the probability for these to be oxidized was estimated to be 2.1% by averaging the oxidation probability of observed methionine residues within the same functional domain. It was determined that $P(1\ \mathrm{ox})$ = 39%, and $P(2\ \mathrm{ox})$ = 19%, indicating that while 39% of the protein may experience secondary oxidation when being incubated in H_2O_2 for longer than 15 min, only 19% of the protein had undergone secondary oxidation at the 15 min oxidation time point. Therefore, the oxidation rate constants determined here may be largely attributed to the oxidation susceptibility of methionine residues within the native CN structure, with only minor contribution from oxidized CN.

The observed CN methionine residues show a wide range in sensitivity toward oxidation with the lowest k_{ox} determined to be 1.5×10^{-6} s^{-1} (Met_{364A}) and the highest k_{ox} of 9.3×10^{-5} s^{-1} (Met_{166B}), as shown in Figure 4, and summarized in Table 1. Interestingly, the methionine residues within the CNA subunit which are highly susceptible to oxidation are all located in the CN regulatory region which includes the CaM binding domain (Met_{406A}), the linker region between the CaM binding and autoinhibitory domains (Met_{431A}), the autoinhibitory domain (Met_{483A}), and the C-terminal (Met_{490A}). The two oxidation sensitive methionine residues within the CNB protein subunit are located in the N-terminal CNA binding domain (Met_{44B}) and at the C-terminus (Met_{166B}). Importantly, Met_{44B} is close to the first Ca^{2+} binding region (31_B-42_B), which is one of the two low-affinity sites that play an important role in CN activation under elevated Ca^{2+} concentrations.[19−21]

It has previously been suggested that oxidation of Met residues located next to cysteine (Cys) residues within the CNA ($Cys_{178A}Met_{179A}$ and $Met_{227A}Cys_{228A}$) and CNB ($Met_{11B}Cys_{12B}$) subunits may facilitate the oxidation of these

dx.doi.org/10.1021/bi5009744 | Biochemistry 2014, 53, 6754−6765

vicinal Cys residues, thereby resulting in attenuation of CN-related activities/functions by compromising the structural integrity of CN.[36,37] However, no experimental evidence was provided to support this hypothesis. Furthermore, although Met_{179A} was not observed in the current study, neither Met_{227A} or Met_{11B} was found to be susceptible to oxidation in the study performed here.

Quantification of Lysine Amino Acid Residue Solvent Accessibility by DMBNHS Modification. To determine whether H_2O_2-induced methionine oxidation resulted in conformational changes within CN, lysine residues within each of the CN samples oxidized at 0, 15, 30, 45, and 60 min time points were modified by reaction with DMBNHS, at DMBNHS/CN molar ratios of 0, 5, 10, 20, 50, and 100. The labeled CN samples were then digested overnight using Glu-C, as modification of lysine residues by DMBNHS would result in missed cleavages at the Lys residue C-termini if trypsin or Lys-C was used. Each digest was then analyzed in triplicate by capillary HPLC-ESI-MS, CID-MS/MS and data-dependent constant neutral loss (DDCNL) triggered CID-MS^3 or ETD-MS/MS. Using this approach, 23 of the total 45 lysine residues within CN were observed, as summarized in Table 2.

Figure 5A,B shows the results from reaction of the native and oxidized (15, 30, 45, and 60 min time points) forms of CN at

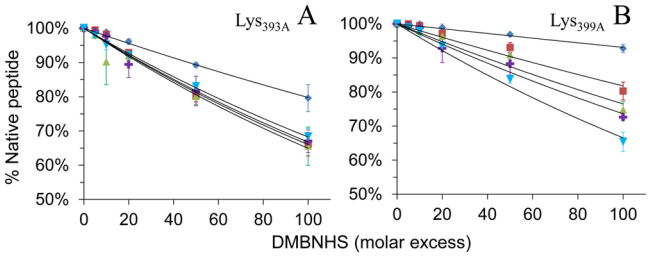

Figure 5. Percentage of unmodified lysine-containing CN peptides observed following reaction with different molar excesses of DMBNHS. (A) Lys_{393A} from 364_A-394_A and (B) Lys_{399A} from 395_A-416_A digested from native CN (♦) and CN oxidized for 15 min (■), 30 min (▲), 45 min (▼), and 60 min (+). All data were run in triplicate and fitted with a single exponential. Error bars are shown as ± standard deviation.

different DMBNHS molar ratios, for the CNA peptides 364_A-394_A (Lys_{393A}) and 395_A-416_A (Lys_{399A}), respectively. From these data, second-order DMBNHS modification rate constants (k_{DMBNHS}) were determined (shown in Table 2 for the 0 and 15 min oxidation time points). As evidenced by the increase in the extent of lysine modification in both peptides as a function of CN oxidation time, the data in Figure 5A,B reveal that both Lys_{393A} and Lys_{399A} underwent conformational changes at the earliest oxidation time point (i.e., 15 min). Longer oxidation times were not found to cause further changes in the region around Lys_{393A} (Figure 5A), whereas Lys_{399A} exhibited further modification with increased oxidation times (Figure 5B), which may result from secondary oxidation-induced conformational changes. The results from all other observed lysine residues are shown in Supplemental Figure S3, Supporting Information. These results indicate that at the 15 min oxidation time point all observed lysine residues exhibited at least some increased reaction with DMBNHS compared to the native nonoxidized form, indicating that the protein complex underwent a global conformational change, or a number of smaller, or more local, conformational changes, upon oxidation. However, most of the observed lysine residues did not undergo significant additional modification with longer oxidation times, indicating that possible secondary oxidation-induced conformational changes were restricted to discrete regions of the protein.

Some peptides contained multiple lysine residues and thus isomeric DMBNHS-modified peptides were generated. Among these, the isomeric forms of modified peptides 34_A-53_A, 394_A-416_A, 419_A-450_A, 451_A-472_A, 457_A-472_A, 75_B-89_B, and 153_B-170_B were all chromatographically resolved. Thus, the modification sites could be identified by CID-MS^3 or ETD-MS/MS and the DMBNHS modification rate constants subsequently determined for each individual lysine residue. However, the isomers of some other modified peptides closely eluted such that the relative abundances for each isomer could not be measured based on their MS ion abundances. In these cases, the relative abundances of the MS/MS fragment ions characteristic for a given modification site were used to calculate the DMBNHS modification rate constant. ETD-MS/MS was favored over CID-MS^3 here for quantification purposes, mainly because of the higher sequence coverage obtained when using the ETD technique. Figure 6 shows the ETD-MS/MS spectrum of the +5 precursor ion charge state of the singly modified CNB peptide 90_B-111_B containing Lys_{91B} and Lys_{103B}, which shows the coexistence of sequence ions corresponding to DMBNHS modification at either amino acid residue. The sum of the ETD-MS/MS ion abundances of all observed fragment ions characteristic of the modification at Lys_{103B} and those characteristic of the modification at Lys_{91B} were used together with the summed MS ion abundances of singly modified 90_B-111_B to obtain the relative abundances of unmodified Lys_{91B} and Lys_{103B}, respectively. The resultant plots used for determination of the second-order DMBNHS modification rate constants are shown in Supplemental Figure S3X,Y, Supporting Information. Using the same method, the DMBNHS modification rate constants were individually quantified for Lys_{424A} and Lys_{441A} from their coeluting 419_A-450_A peptides (Supplemental Figure S4, Supporting Information). However, due to the low abundance of the singly modified 419_A-450_A peptide when CN was modified using a low molar excess of DMBNHS, and subsequently the low abundance of the ETD-MS/MS product ions, the DMBNHS modification rate constants for these residues were only calculated from the 20-, 50-, and 100-fold DMBNHS molar excess reaction conditions. For peptides containing more than two modifiable sites, such as CNB peptide 19_B-42_B, containing Lys_{21B}, Lys_{25B}, Lys_{28B}, and Lys_{29B}, DMBNHS modification rate constants could only be quantified for the first and last lysine residue within the peptide (i.e., Lys_{21B} and Lys_{29B}). However, as unambiguous characteristic ETD-MS/MS product ions could not be observed for Lys_{29B} (Supplemental Figure S5, Supporting Information), the DMBNHS modification rate constant was determined only for Lys_{21B}. It is important to point out that the rate constants determined from the abundances of the ETD-MS/MS product ions are not correlated with the actual extent of DMBNHS modification, as the abundances of product ions are affected by a variety of factors, including differences in ionization efficiency and ETD cleavage bias, between the unmodified and modified peptides. However, the variance in product ion intensities induced by these factors should be consistent from run to run when the same peptides are analyzed. Therefore, the fold change in DMBNHS modification rate constants upon oxidation (see below) can be considered indicative of the extent of

dx.doi.org/10.1021/bi5009744 | Biochemistry 2014, 53, 6754−6765

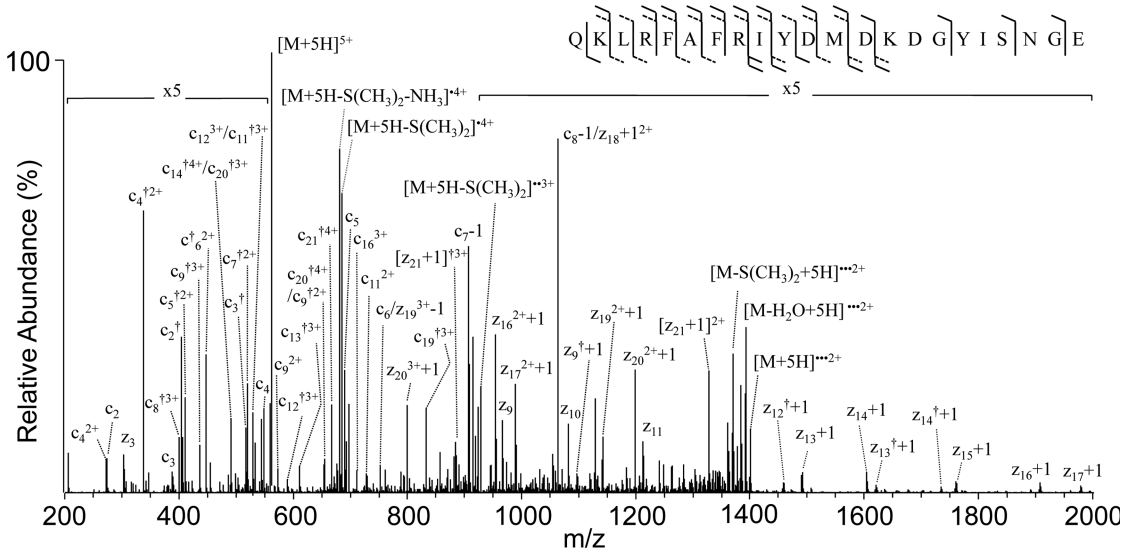

Figure 6. ETD-MS/MS characterization of coeluting isomers of the +5 precursor ion of singly modified 90_B-111_B containing either modified Lys_{91B} or modified Lys_{103B}. A superscript † indicates sequence ions containing one DMBNHS-modified amino acid residue. A dashed line in the sequence indicates an unoxidized sequence ion was observed, while a solid line indicates that a singly oxidized sequence ion was observed.

conformational change occurring within specific regions of the CN protein complex.

It was interesting to notice that the DMBNHS modification rate constants for Lys_{459A} and Lys_{466A} determined from the native CN Glu-C digest peptide 451_A-472_A (k_{DMBNHS} of Lys_{459A} = 8.9 × 10^{-7} M^{-1} s^{-1} and Lys_{466A} = 1.4 × 10^{-6} M^{-1} s^{-1}) were lower than those determined from the 457_A-472_A peptide within the same digest (k_{DMBNHS} of Lys_{459A} = 1.4 × 10^{-6} M^{-1} s^{-1} and k_{DMBNHS} of Lys_{466A} = 1.7 × 10^{-6} M^{-1} s^{-1}). Similar differences were observed between the 451_A-472_A and 457_A-472_A peptides from the oxidized CN protein (Table 2). One possible explanation for this is that the incorporation of the fixed charge sulfonium ion could enhance enzymatic cleavage when the cleavable site is close to the modification site. Also, the enhancement of ionization efficiency caused by the incorporation of the fixed charge is expected to affect shorter peptides more than longer peptides.[31,32] However, no apparent difference in DMBNHS modification rate constants was observed between other peptides, e.g., 364_A-394_A and 373_A-394_A, both containing Lys_{393A}. This is expected as DMBNHS modification of Lys_{393A} could only affect the efficiency of the cleavage at the C-terminal of Glu_{394A} of both peptides. Furthermore, incorporation of only one fixed charge to this peptide would not be expected to enhance the ionization efficiency to the same degree as the incorporation of two fixed charges.

Despite the observed variations in DMBNHS modification rates caused by digestion and/or ionization efficiency, the overall fold change in DMBNHS modification rate constants (described below) used to quantify conformational changes between the native and oxidized forms of CN remained consistent among different peptides containing the same lysine residues. For example, after being oxidized for 15 min, the fold changes determined for the DMBNHS modification rate constant of Lys_{459A} from peptide 451_A-472_A and 457_A-472_A were 1.44 and 1.54-fold, respectively, with a standard deviation of 0.08.

The extent of CN conformational change upon oxidation was characterized by dividing the DMBNHS modification rate constant of each observed lysine residue from the oxidized (15 min time point) CN protein complex by the DMBNHS modification rate constant of the same lysine residue from the native CN protein complex, yielding a fold change indicative of each lysine residue's DMBNHS modification rate constant as a function of oxidation (Figure 7). Data labels in Figure 7

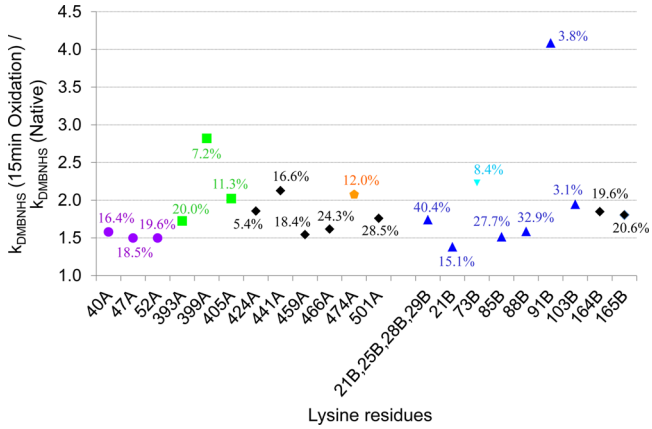

Figure 7. Ratio of second-order DMBNHS modification rate constants determined for observed lysine residues from oxidized CN (15 min reaction time point) over the DMBNHS modification rate constants determined for the corresponding Lys residues from native CN. CN Lys residues located in the catalytic domain (purple solid circle), CaM binding domain (green solid box) and autoinhibitory region (orange solid pentagon) of CNA, the CNA binding region (blue solid up triangle) and Ca^{2+} binding domain (light blue solid down triangle) of CNB and nonfunctional regions (♦). Data labels indicate the percent modification observed in the native CN protein complex at a DMBNHS molar excess of 100.

indicate the percent modification for each lysine residues that was observed in the native CN protein complex using a DMBNHS molar excess of 100. When the same lysine residue was observed from different peptides, the DMBNHS modification rate constants determined from all observed peptides were averaged and then used to calculate the fold increase.

dx.doi.org/10.1021/bi5009744 | Biochemistry 2014, 53, 6754−6765

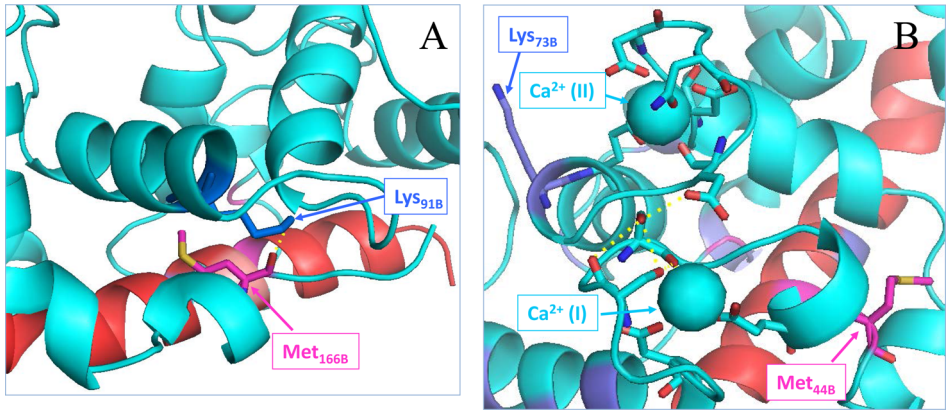

Figure 8. Structural illustration of the correlation (A) between Lys_{91B} and Met_{166B} and (B) between Lys_{73B} and Met_{44B}, based on the crystal structure of human calcineurin (PDB entry: 1AUI). The CNA and CNB sequences are illustrated in red and cyan, respectively. Lys_{91B} and Lys_{73B} are shown as blue sticks, while Met_{166B} and Met_{44B} are shown as pink sticks. Ca^{2+} ions are illustrated as cyan spheres. Residues that interact with Ca^{2+} in the Ca^{2+} binding pockets are shown as cyan sticks. Hydrogen bonds are illustrated as yellow dashed lines.

Lysine residues that showed greater than a 2-fold increase in their modification rate constants were found to be located in (i) the CaM binding domain (Lys_{399A} and Lys_{405A}), (ii) the linker region between CaM binding and AI domains (Lys_{441A}), (iii) the AI domain (Lys_{474A}) of CNA, and (iv) the Ca^{2+} binding regions (Lys_{73B}), and (v) the CNA binding region (Lys_{91B}) of CNB. Thus, similar to the locations of oxidation sensitive methionine residues, the lysine residues that showed significant increases in k_{DMBNHS} between the oxidized and native proteins are located in CN domains involved in Ca^{2+}/CaM binding and stimulation.

Lys_{91B} showed the largest fold increase in k_{DMBNHS} upon oxidation. Interestingly, in the crystal structure of CN,[7] the ε-amino group of Lys_{91B} is hydrogen-bonded to the amide carbonyl group of Met_{166B} (Figure 8A), i.e., the methionine residue that exhibited the highest susceptibility toward oxidation (see Figure 4). Thus, we propose that oxidation of Met_{166B} disrupts the local hydrogen bonding environment between Met_{166B} and Lys_{91B}, exposing the ε-amino group of Lys_{91B} to increased DMBNHS modification. Notably, both Met_{166B} and Lys_{91B} are located in the CNA−CNB interface region. Conformational changes in this area may therefore impair the interaction between CNA and CNB. It has been reported previously that CNB binding can also stimulate CN, although to a less extent compared to CaM.[38] Also, CNB interaction has been demonstrated to facilitate CaM regulated CN activation.[21,39] Therefore, perturbed interactions between CNA and CNB may contribute to the decrease of CN activity upon oxidative modification.

Lys_{73B} also showed a relatively large fold change in DMBNHS modification rate constant upon oxidation (2.2-fold increase). No methionine residues are sequentially or spatially close to Lys_{73B} (Figure 8B). However, conformational changes surrounding the Lys_{73B} residue may result from oxidation of one or several remote methionine residue(s) within the same region of the protein. One possible remote oxidation site is Met_{44B}, which was also determined to be highly susceptible to oxidation (Figure 4) in the CNB protein subunit. Oxidation of Met_{44B}, which is located close to the first Ca^{2+} binding pocket (31_B-42_B), may induce a conformational change in the second Ca^{2+} binding pocket (63_B-74_B), which involves Lys_{73B}, as these two Ca^{2+} binding pockets are hydrogen-bonded to each other (Figure 8B). Upon being saturated with Ca^{2+}, these two N-terminal low-affinity Ca^{2+} binding sites have been demonstrated to activate CN by direct CNB/CNA interaction and by facilitating CaM/CNA binding.[8,21] Therefore, conformational change in these two Ca^{2+} binding sites may cause impaired Ca^{2+} binding to CNB, which may further inhibit CNB or/and CaM regulated CN stimulation.

Lys_{399A} and Lys_{405A}, located within the CaM binding domain of CNA, also showed greater than 2-fold increases in their DMBNHS modification rate constants upon CN oxidation. Met_{406A} is directly adjacent to Lys_{405A}, so it is reasonable to expect that oxidation of this residue (which was determined to be susceptible toward oxidation; see Figure 4), would affect the chemical environment around Lys_{405A}. No methionine residues are close to Lys_{399A} in the CN sequence. Unfortunately, neither Lys_{399A} nor Lys_{405A} is visible in the known crystal structure of CN, so methionine residues that are spatially close to these residues in the folded tertiary structure cannot be determined. Nonetheless, conformational changes resulting from oxidation, subsequently reflected by increased Lys_{399A} and Lys_{405A} DMBNHS reactivity, that are both located within the CaM binding domain, may directly impair CN/CaM binding and inhibit CN activation.

Lys_{441A}, residing in the linker region between the CaM binding and AI domains, showed a 2.1-fold increase in k_{DMBNHS} upon oxidation. However, as Lys_{441A} is also not visible in the known crystal structure of CN, the methionine residues whose oxidation may cause the conformational change to the region around this residue cannot be identified. However, oxidation of Met_{431A}, which is located within the AI domain and has been determined to be highly susceptible toward oxidation (see Figure 4) may induce a conformational change in the sequentially close region around Lys_{441A}. Furthermore, it has been demonstrated that CaM binding induces extensive folding not only within the CaM binding domain but also contributes to maintaining the AI domain in the active configuration.[8−10] Therefore, it is plausible to propose that a structural alteration in the linker region may prohibit the displacement of AI from the active site upon CaM binding. Also, it is possible that a conformational change in the CaM binding domain might induce a perturbation to the linker region between the CaM binding and the AI domains, and vice versa.

The lysine residue in the AI domain, Lys_{474A}, also exhibited a DMBNHS modification rate constant increase greater than 2-

dx.doi.org/10.1021/bi5009744 | *Biochemistry* 2014, 53, 6754−6765

fold, indicating a conformational change within the AI domain upon CN oxidation that could hinder displacement of the AI domain from the catalytic site upon Ca^{2+}/CaM binding. Also, CaM binding induced displacement of the AI domain from the catalytic center involves an extensive conformational change in the regulatory region ranging from the CaM binding domain to the AI domain. Therefore, oxidation-induced conformational changes that occurred within the CaM binding domain and the linker region between the CaM binding and AI domains may also have a negative effect on displacement of the AI domain from the catalytic center upon CaM binding, thereby contributing to CN inactivation. Met_{483A}, located in the AI domain, and Met_{490A}, located close to the AI domain, both exhibited high susceptibility toward oxidation. However, it is not clear whether oxidation of these residues was the cause of conformational change in the region around Lys_{474A}, as no methionine residues observable in the crystal structure of CN are found to be in direct contact with Lys_{474A}.

CONCLUSIONS

Using a novel derivatization reagent and mass spectrometry based analysis strategy to monitor changes in the covalent modification rates of lysine residues between native and H_2O_2-induced oxidized forms of CN, multiple regions within the protein complex that undergo significant conformational perturbation upon oxidative modification have been identified. Importantly, both the methionine residues found to be highly susceptible toward oxidation, and the lysine residues exhibiting large increases in accessibility upon oxidation, were all located in calcineurin functional domains involved in Ca^{2+}/CaM binding regulated calcineurin stimulation. Therefore, the results obtained in this study provide support for the hypothesis that H_2O_2-induced methionine oxidation results in global and/or localized conformational changes that contribute to CN inactivation, by impairing the interaction between CNA and CNB, Ca^{2+} and CNB, or/and CaM and CNA, or/and by altering the affinity between AI and the catalytic center.

ASSOCIATED CONTENT

Supporting Information

Supplemental Figure S1. Ion trap CID-MS/MS of the triply protonated precursor ion isomers of the singly oxidized Arg482A-Glu506A peptide containing (A) oxidized Met490A and (B) oxidized Met483A. Percentage of Met containing CN peptides from the Glu-C digest, trypsin digest, and Lys-C digest remaining in a native form following treatment with 12 mM H_2O_2. Supplemental Figure S3. Plots of the relative abundances of unmodified Lys residues versus the molar ratios of DMBNHS over CN, digested from native CN, CN oxidized for 15 min, 30 min, 45 min, and 60 min. Supplemental Figure S4. ETD-MS/MS characterization of the co-eluting isomers of the +4 precursor ion of the singly modified Ser419A-Glu450A peptide, containing either modified Lys424A or modified Lys441A. Supplemental Figure S5. ETD-MS/MS characterization of the co-eluting isomers of the +4 precursor ion of the singly modified Ile19B-Glu42B peptide containing either modified Lys21B, Lys25B, Lys28B, or Lys29B. Supplemental Table S1. Summary of data-dependent constant neutral loss (DDCNL) MS/MS values employed for the identification of DMBNHS-modified Glu-C digest peptides from calcineurin. This material is available free of charge via the Internet at http://pubs.acs.org.

AUTHOR INFORMATION

Corresponding Author

*Current address: School of Chemistry, Department of Biochemistry and Molecular Biology, Bio21 Molecular Science and Biotechnology Institute, The University of Melbourne, 30 Flemington Rd, Room 431, Parkville Victoria 3010, Australia. Phone +61 3 8344 2650. E-mail: gavin.reid@unimelb.edu.au.

Funding

This study was supported by funding from NSF CHE-0547940 to GER, and from NIH P30 CA022453 and NIH P30 ES020957 to P.M.S.

Notes

The authors declare no competing financial interest.

ACKNOWLEDGMENTS

We thank Namhee Shin from Wayne State University for the preparation of calcineurin used in this study.

REFERENCES

(1) Rusnak, F., and Mertz, P. (2000) Calcineurin: Form and Function. *Physiol. Rev. 80*, 1483−1521.

(2) Schulz, R. A., and Yutzey, K. E. (2004) Calcineurin Signaling and NFAT Activation in Cardiovascular and Skeletal Muscle Development. *Dev. Biol. 266*, 1−16.

(3) Sakuma, K., and Yamaguchi, A. (2010) The Functional Role of Calcineurin in Hypertrophy, Regeneration, and Disorders of Skeletal Muscle. *J. Biomed. Biotechnol. 2010*, 721219.

(4) Mallinson, J., Meissner, J., and Chang, K. C. (2009) Chapter 2. Calcineurin Signaling and the Slow Oxidative Skeletal Muscle Fiber Type. *Int. Rev. Cell Mol. Biol. 277*, 67−101.

(5) Agrawal, R., Agrawal, N., Koyani, C. N., and Singh, R. (2010) Molecular Targets and Regulators of Cardiac Hypertrophy. *Pharmacol. Res. 61*, 269−280.

(6) Fujiwara, A., Kakizawa, S., and Eno, M. (2007) Induction of Cerebellar Long-Term Depression Requires Activation of Calcineurin in Purkinje Cells. *Neuropharmacology 52*, 1663−1670.

(7) Kissinger, C. R., Parge, H. E., Knighton, D. R., Lewis, C. T., Pelletier, L. A., Tempczyk, A., Kalish, V. J., Tucker, K. D., Showalter, R. E., Moomaw, E. W., Gastinel, L. N., Habuka, N., Chen, X. H., Maldonado, F., Barker, J. E., Bacquet, R., and Villafranca, J. E. (1995) Crystal-Structures of Human Calcineurin and the Human Fkbp12-Fk506-Calcineurin Complex. *Nature 378*, 641−644.

(8) Shen, X., Li, H., Ou, Y., Tao, W., Dong, A., Kong, J., Ji, C., and Yu, S. (2008) The Secondary Structure of Calcineurin Regulatory Region and Conformational Change Induced by Calcium/Calmodulin Binding. *J. Biol. Chem. 283*, 11407−11413.

(9) Rumi-Masante, J., Rusinga, F. I., Lester, T. E., Dunlap, T. B., Williams, T. D., Dunker, A. K., Weis, D. D., and Creamer, T. P. (2012) Structural Basis for Activation of Calcineurin by Calmodulin. *J. Mol. Biol. 415*, 307−317.

(10) Dunlap, T. B., Cook, E. C., Rumi-Masante, J., Arvin, H. G., Lester, T. E., and Creamer, T. P. (2013) The distal helix in the regulatory domain of calcineurin is important for domain stability and enzyme function. *Biochemistry. 52*, 8643−8651.

(11) King, M. M., and Huang, C. Y. (1984) The Calmodulin-Dependent Activation and Deactivation of the Phosphoprotein Phosphatase, Calcineurin, and the Effect of Nucleotides, Pyrophosphate, and Divalent Metal-Ions - Identification of Calcineurin as a Zn and Fe Metalloenzyme. *J. Biol. Chem. 259*, 8847−8856.

(12) Yu, L., Haddy, A., and Rusnak, F. (1995) Evidence That Calcineurin Accommodates an Active-Site Binuclear Metal Center. *J. Am. Chem. Soc. 117*, 10147−10148.

(13) Griffith, J. P., Kim, J. L., Kim, E. E., Sintchak, M. D., Thomson, J. A., Fitzgibbon, M. J., Fleming, M. A., Caron, P. R., Hsiao, K., and Navia, M. A. (1995) X-Ray Structure of Calcineurin Inhibited by the

Immunophilin Immunosuppressant Fkbp12-Fk506 Complex. *Cell 82*, 507−522.
(14) Yu, L., Golbeck, J., Yao, J., and Rusnak, F. (1997) Spectroscopic and Enzymatic Characterization of the Active Site Dinuclear Metal Center of Calcineurin: Implications for a Mechanistic Role. *Biochemistry 36*, 10727−10734.
(15) Bogumil, R., Namgaladze, D., Schaarschmidt, D., Schmachtel, T., Hellstern, S., Mutzel, R., and Ullrich, V. (2000) Inactivation of Calcineurin by Hydrogen Peroxide and Phenylarsine Oxide - Evidence for a Dithiol-Disulfide Equilibrium and Implications for Redox Regulation. *Eur. J. Biochem. 267*, 1407−1415.
(16) Oin, K. F., Khangulov, S., Liu, C., and Huang, C. Y. (1995) Role of Fe Ion in Calcineurin Studied by Erp and Activity Measurements. *FASEB J. 9*, A1347−A1347.
(17) Namgaladze, D., Hofer, H. W., and Ullrich, V. (2002) Redox Control of Calcineurin by Targeting the Binuclear Fe^{2+}-Zn^{2+} Center at the Enzyme Active Site. *J. Biol. Chem. 277*, 5962−5969.
(18) Aitken, A., Klee, C. B., and Cohen, P. (1984) The Structure of the B-Subunit of Calcineurin. *Eur. J. Biochem. 139*, 663−671.
(19) Gallagher, S. C., Gao, Z.-H., Li, S., Dyer, R. B., Trewhella, J., and Klee, C. B. (2001) There is Communication between all Four Ca^{2+}-Bindings Sites of Calcineurin B. *Biochemistry 40*, 12094−12102.
(20) Yang, S.-A., and Klee, C. B. (2000) Low Affinity Ca^{2+}-Binding Sites of Calcineurin B Mediate Conformational Changes in Calcineurin A. *Biochemistry 39*, 16147−16154.
(21) Stemmer, P. M., and Klee, C. B. (1994) Dual Calcium Ion Regulation of Calcineurin by Calmodulin and Calcineurin B. *Biochemistry 33*, 6859−6866.
(22) Filosto, S., Fry, W., Knowlton, A. A., and Goldkorn, T. (2010) Neutral Sphingomyelinase 2 (nSMase2) is a Phosphoprotein Regulated by Calcineurin (PP2B). *J. Biol. Chem. 285*, 10213−10222.
(23) Wang, X. T., Culotta, V. C., and Klee, C. B. (1996) Superoxide Dismutase Protects Calcineurin from Inactivation. *Nature 383*, 434−437.
(24) Sommer, D., Fakata, D. L., Swanson, S. A., and Stemmer, P. M. (2000) Modulation of the Phosphatase Activity of Calcineurin by Oxidants and Antioxidants *in vitro*. *Eur. J. Biochem. 267*, 2312−2322.
(25) Reiter, T. A., Abraham, R. T., Choi, M., and Rusnak, F. (1999) Redox Regulation of Calcineurin in T-Lymphocytes. *J. Biol. Inorg. Chem. 4*, 632−644.
(26) Namgaladze, D., Shcherbyna, L., Kienhofer, J., Hofer, H. W., and Ullrich, V. (2005) Superoxide Targets Calcineurin Signaling in Vascular Endothelium. *Biochem. Biophys. Res. Commun. 334*, 1061−1067.
(27) Carruthers, N. J., and Stemmer, P. M. (2008) Methionine Oxidation in the Calmodulin-Binding Domain of Calcineurin Disrupts Calmodulin Binding and Calcineurin Activation. *Biochemistry 47*, 3085−3095.
(28) Mendoza, V. L., and Vachet, R. W. (2009) Probing Protein Structure by Amino Acid-Specific Covalent Labeling and Mass Spectrometry. *Mass Spectrom. Rev. 28*, 785−815.
(29) Konermann, L., Stocks, B. B., Pan, Y., and Tong, X. (2010) Mass Spectrometry Combined with Oxidative Labeling for Exploring Protein Structure and Folding. *Mass Spectrom. Rev. 29*, 651−667.
(30) Jones, L. M., B. Sperry, J., A. Carroll, J., and Gross, M. L. (2011) Fast Photochemical Oxidation of Proteins for Epitope Mapping. *Anal. Chem. 83*, 7657−7661.
(31) Zhou, X., Lu, Y., Wang, W., Borhan, B., and Reid, G. E. (2010) 'Fixed Charge' Chemical Derivatization and Data Dependant Multistage Tandem Mass Spectrometry for Mapping Protein Surface Residue Accessibility. *J. Am. Soc. Mass Spectrom. 21*, 1339−1351.
(32) Lu, Y., Zhou, X., Stemmer, P., and Reid, G. (2012) Sulfonium Ion Derivatization, Isobaric Stable Isotope Labeling and Data Dependent CID- and ETD-MS/MS for Enhanced Phosphopeptide Quantitation, Identification and Phosphorylation Site Characterization. *J. Am. Soc. Mass Spectrom. 23*, 577−593.
(33) Fraczkiewicz, R., and Braun, W. (1998) Exact and Efficient Analytical Calculation of the Accessible Surface Areas and Their Gradients for Macromolecules. *J. Comput. Chem. 19*, 319−333.
(34) Reid, G. E., Roberts, K. D., Kapp, E. A., and Simpson, R. J. (2004) Statistical and Mechanistic Approaches to Understanding the Gas-Phase Fragmentation Behavior of Methionine Sulfoxide Containing Peptides. *J. Proteome Res. 3*, 751−759.
(35) Srikanth, R., Wilson, J., Bridgewater, J., Numbers, J., Lim, J., Olbris, M., Kettani, A., and Vachet, R. (2007) Improved Sequencing of Oxidized Cysteine and Methionine Containing Peptides Using Electron Transfer Dissociation. *J. Am. Soc. Mass Spectrom. 18*, 1499−1506.
(36) Agbas, A., and Moskovitz, J. (2009) The Role of Methionine Oxidation/Reduction in the Regulation of Immune Response. *Curr. Signal Transduct. Ther. 4*, 46−50.
(37) Agbas, A., Zaidi, A., and Michaelis, E. K. (2005) Decreased activity and increased aggregation of brain calcineurin during aging. *Brain Res. 1059*, 59−71.
(38) Stewart, A. A., Ingebritsen, T. S., Manalan, A., Klee, C. B., and Cohen, P. (1982) Discovery of a Ca^{2+}-and Calmodulin-Dependent Protein Phosphatase. *FEBS Lett. 137*, 80−84.
(39) Perrino, B. A., Fong, Y. L., Brickey, D. A., Saitoh, Y., Ushio, Y., Fukunaga, K., Miyamoto, E., and Soderling, T. R. (1992) Characterization of the Phosphatase Activity of a Baculovirus-Expressed Calcineurin A Isoform. *J. Biol. Chem. 267*, 15965−15969.